Article

Micromechanical Analysis of a Bio-Sandwich Application for Cylinder under Pressure

Ghania Habbar [1], Abdelhakim Maizia [1], Abdelkader Hocine [1], João Ribeiro [2,3,*] and Mohamed Houcine Dhaou [4,5]

1   Controls Laboratory Tests, Measurements and Simulations Mechanics, Hassiba Benbouali University of Chlef, Hay Salem, P.O. Box 151, Chlef 02180, Algeria; g.habbar93@univ-chlef.dz (G.H.); a.maizia@univ-chlef.dz (A.M.); a.hocine@univ-chlef.dz (A.H.)
2   Higher School of Technology and Management, Instituto Politécnico de Bragança, 5300-252 Braganca, Portugal
3   Mountain Research Centre, Instituto Politécnico de Bragança, 5300-252 Braganca, Portugal
4   Department of Physics, College of Science, Qassim University, Buraydah 51452, Saudi Arabia; m.dhaou@qu.edu.sa
5   Laboratory of Thermal and Energetic Systems Studies (LESTE), National School of Engineering of Monastir, University of Monastir, Monastir 5000, Tunisia
*   Correspondence: jribeiro@ipb.pt

Abstract: In recent years, there has been a growing replacement of synthetic fibers by natural ones, particularly by autochthonous materials. In the case of Algeria, the most abundant plant resources are the PALF (Pineapple leaf fiber), the date palm, and the Alfa fibers. In this work, the development and use of analytical and numerical methods are proposed to predict the mechanical properties of layers based on natural fibers that will be applied to manufacture skins of the sandwich cylinder. To achieve these predictions, four analytical models were used, namely the Halpin–Tsai, the Chamis, the Hashin vs. Rosen, and the ROM. The analytical results were compared with the numerical simulations and experimental data. The prediction of the elastic properties of the three fiber-based eco-composites showed an important dispersion in terms of stiffness.

Keywords: natural fibers; skin layer; Bio-Sandwich; FEM; analytical methods; micromechanical

1. Introduction

The composites' materials have low weight, high rigidity, and excellent energy absorption, making them ideal for structural applications compared to traditional materials [1,2]. A typical sandwich structure is one of the configurations of composite materials; it consists of two face sheets separated by a lightweight, thick core structure constructed of foam or honeycombs [3]. Sandwich cores are available in a variety of shapes and materials, including honeycomb and metals for aerospace, marine, piping, and vessel applications, depending on industry standards and functional needs [4].

Sandwich pipes for vessel storage are multilayered, comprised of multiple lightweight, synthetic fiber skins fully bonded to a polymeric core. They are an especially attractive concept because of their high strength, stiffness-to-weight ratios, and corrosion resistance [5,6].

The synthetic fibers, which are used in the fabrication of the skin sandwich, have many disadvantages: they are far less biodegradable and have less desirable cost and availability in comparison with natural fibers [7].

Several research studies focus on the replacement of synthetic skins by eco-composites based on natural fibers [8–10] in a sandwich structure, such as palm, kenaf, banana, ramie, jute, leaf spring, flax, hemp, pineapple, and Alfa [11–18]. This interest is justified because of their widespread availability, lightness, strength [19,20], biodegradability, sustainable and renewable nature [21,22], in addition to their high specific modulus and low cost [16,23], low wear of tooling, skin irritation, and environmentally-friendliness [24,25]. Natural

fiber composites, as opposed to synthetic fiber composites, may provide more effective recycling solutions due to their bio-based feedstock and capacity to generate additional energy during incineration [23,26]. Bio-based composites appear to be very promising alternatives to traditional composites, as they have lower densities and, as a result, particular property/density ratios comparable to glass fibers [27]. These properties reveal a new horizon for researchers to replace the synthetic fiber reinforcements in composites [28].

Before achieving the sizing of the tubular eco-sandwich cylinder, a multiscale characterization is performed, beginning with the micro and macro-mechanical scales. The micromechanical approach (part 1) is used to predict the mechanical properties of bio skins. Before analyzing the whole cylinder sandwich structure under different loading, the second step focuses on understanding the behavior of a sandwich element in the tubular structure through a macro-mechanical model (part 2).

A large number of Finite Element Models (FEM) and analytical micromechanical models have been proposed in the literature for predicting various mechanical properties of composite materials [29–32]. For the FEM model, the representative volume elements (RVE) of bio-composites were established in different software, such as ANSYS, ABAQUS, and DIGIMAT [30–32], to determine the micromechanical properties and failure mechanism of bio-composites. Currently, many researchers are attempting to anticipate the natural fiber polymer composite's mechanical performance using various mathematical and numerical methods. The rule of mixtures (ROM), inverted ROM (IROM), Halpin–Tsai model, Cox model, Kelly–Tyson model [32], and Mori–Tanaka model [33–36] are the most widely used and well-known theories for defining mechanical characteristics. In addition, several additional models, such as the bridging model, Hashin and Rosen, Double-Inclusion model [37], Christensen equation, and Chamis model, have been used to determine the mechanical properties of composite materials.

This first part of the contribution aims to predict the mechanical properties of skin layers made from PALF (Pineapple leaf fiber), date palm, and Alfa fibers, which are among Algeria's most abundant plant resources, at different volume fractions. To this end, micromechanical analytical and FEM models have been developed under MATLAB 8.3 and ANSYS 18.1 software. The influence of the volume fraction of reinforcement on Young's and shear modulus and Poisson's ratios is studied.

The analytical models are based on four theories, Halpin–Tsai, Chamis, Hashin vs. Rosen, and ROM. To choose a suitable theory from them that is in good agreement with the experimental data obtained by Rakesh [13], a comparison is made for the composite made from PALF fibers.

The suitable theory is used with the FEM model to predict the mechanical properties of skin layers made from PALF, date palm, and Alfa fibers, where the results are inefficient in combination. The FEM used four RVE, depending on the volume fraction of natural fibers.

2. Materials and Methods

The different material properties of both the matrix and fiber are shown in Table 1. By altering the volume fraction of the fiber, material properties are utilized to establish the mechanical properties of the composites, which are the longitudinal Young's modulus (E_{11}), transverse Young's modulus (E_{22}), longitudinal shear modulus (G_{12}), and major Poisson's ratio (v_{12}).

Table 1. Properties of the constituents.

Material	Young's Modulus [GPa]	Poisson's Ratio	Reference
Epoxy	3.75	0.35	[13]
PALF	29.3	0.30	
DB date palm tree fiber	6.63	0.152	[38]
Alfa fiber	19.77	0.34	[39]

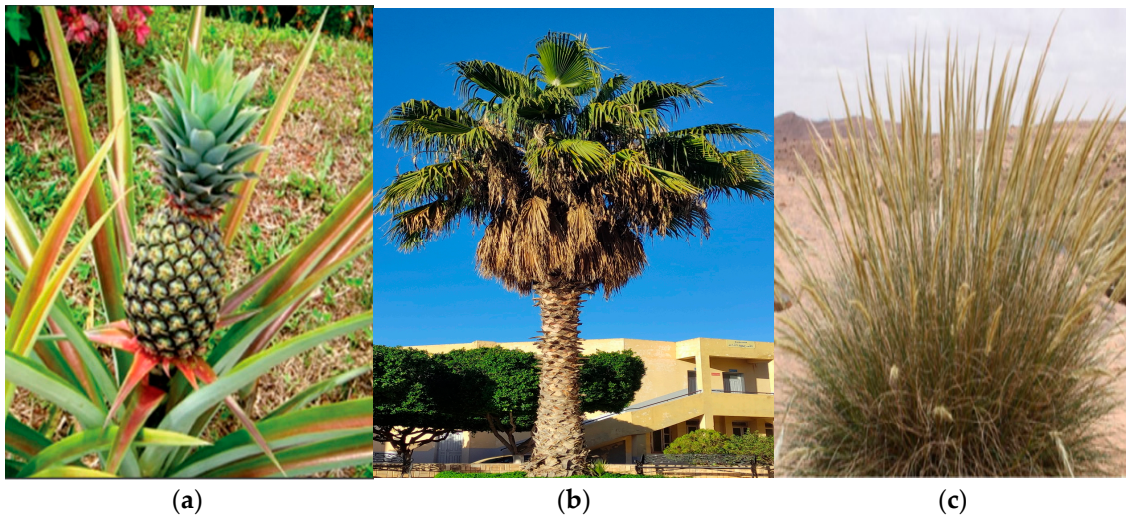Figure 1 shows the different natural fiber plants used in this paper.

Figure 1. Natural fiber plants: (**a**) Pineapple [40], (**b**) Palm and (**c**) Alfa [12].

2.1. Analytical Analysis

Many studies have focused on predicting the mechanical properties of composites. To evaluate the elastic properties of composites, different micromechanical models have been proposed, such as the Halpin–Tsai model, the Chamis model, the rule of mixtures (ROM), and the Hashin and Rosen model. The analytical models were derived from [41]. The equations of these four models are written as:

- Halpin–Tsai model

$$E_{11} = E_F V_F + E_M V_M \tag{1}$$

$$v_{12} = v_F V_F + v_M V_M \tag{2}$$

$$E_{22} = E_M \cdot \left(\frac{1 + \zeta_\eta \cdot V_F}{1 - \eta V_F} \right) \quad \text{with}: \quad \eta = \left(\frac{\left[\frac{E_F}{E_M} \right] - 1}{\left[\frac{E_F}{E_M} \right] + \zeta} \right) \tag{3}$$

$$G_{12} = G_M \left(\frac{1 + \zeta_\eta \cdot V_F}{1 - \eta V_F} \right) \tag{4}$$

- Chamis model

$$E_{11} = V_F E_F + V_M E_M \tag{5}$$

$$E_{22} = \frac{E_M}{1 - \sqrt{V_F}(1 - E_M/E_F)} \tag{6}$$

$$v_{12} = V_F v_F + V_M v_M \tag{7}$$

$$G_{12} = \frac{G_M}{1 - \sqrt{V_F}\,(1 - G_M/G_F)} \tag{8}$$

- ROM model

$$E_{11} = V_F E_F + V_M E_M \tag{9}$$

$$E_{22} = \frac{E_F E_M}{E_M \cdot V_F + E_F \cdot V_M} \tag{10}$$

$$v_{12} = V_F v_F + V_M v_M \tag{11}$$

$$G_{12} = \frac{G_F \cdot G_M}{G_F \cdot V_M + G_M \cdot V_F} \tag{12}$$

- Hashin and Rosen model

$$E_{11} = V_F E_F + V_M E_M + \frac{4 V_F V_M (v_F - v_M)^2}{\frac{V_F}{K_M} + \frac{1}{G_M} + \frac{V_M}{K_F}} \tag{13}$$

$$E_{22} = 2(1 + v_{23}) \cdot G_{23} \tag{14}$$

$$v_{12} = V_F \cdot v_F + V_M \cdot v_M + \frac{V_F V_M (v_F - v_M)\left(\frac{1}{K_M} - \frac{1}{K_F}\right)}{\frac{V_F}{K_M} + \frac{1}{G_M} + \frac{V_M}{K_F}} \tag{15}$$

$$G_{12} = G_M \cdot \frac{G_F(1 + V_F) + G_M \cdot V_M}{G_F \cdot V_M + G_M(1 + V_F)} \tag{16}$$

where: E_{11} Longitudinal Young's modulus; E_M Young's Modulus of Matrix; E_F Young's Modulus of Fiber; V_F Volume fraction of fiber; E_{22} Transverse Young's modulus; Lateral pressure module; $G_{TT'}$ Transverse shear module; v_{12} Major Poisson's ratio; v_F Poisson's ratio of fiber; v_M Poisson's Ratio of Matrix; G_{12} Longitudinal shear modulus; G_F Shear modulus of fiber; G_M Shear modulus of matrix; K_F Lateral compression module of fiber; K_M Lateral compression module of matrix; ζ is called the reinforcing factor.

2.2. FEM Analysis

2.2.1. Fiber-Reinforced Composite Numerical Homogenization

Epoxy and one of the fibers (PALF, Palm fiber, or Alfa fiber) are the main components of the Particle Reinforced Composite. To accomplish the analysis, the homogenization approach is used for a fiber-reinforced composite by selecting continuous fibers as reinforcement. Figure 2 illustrates a uniform distribution of fiber in the epoxy, by using the finite element software ANSYS 18.1 to solve the problem.
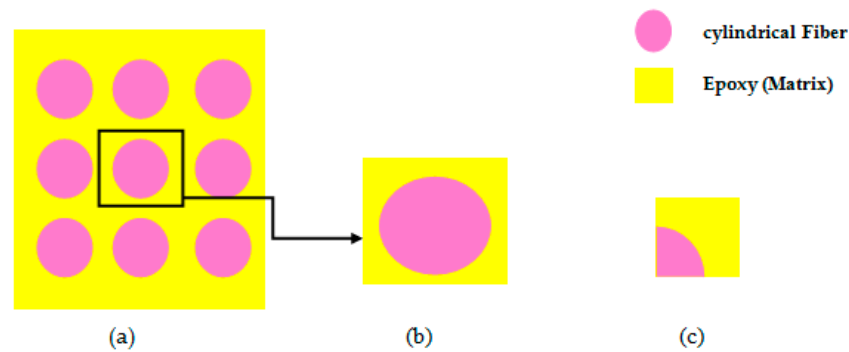

Figure 2. (**a**) Uniform distribution of fibers in the matrix; (**b**) Isolated Unit cell; (**c**) One-eighth Model.

2.2.2. Element Type

The ANSYS SOLID 186 element [42] is shown in Figure 3, which is a higher-order 3D 20-node solid element with quadratic displacement behavior, was used in this study. There are 20 nodes in the element, each with three degrees of freedom (DOF) (translations in the three nodal directions).
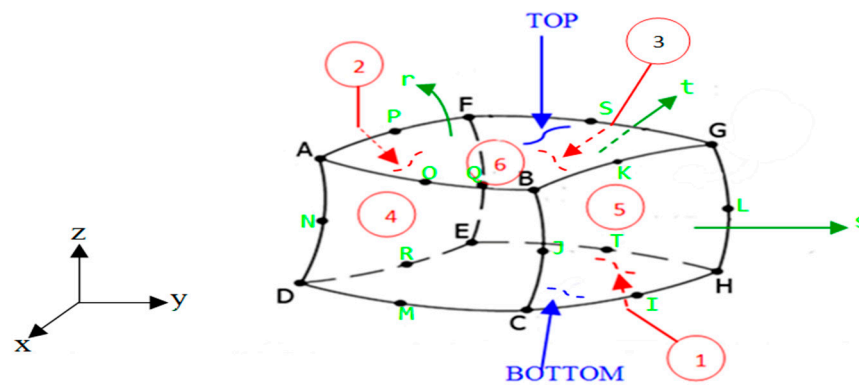
Figure 3. The element used for meshing the finite element models.

2.2.3. Geometry and Finite Element Modeling

The representative volume element (RVE) used for the hybrid analysis has the form of a square cube. Due to the symmetry in geometry, loading, and boundary conditions, only one-fourth of the RVE's cross-section is modeled and studied. As one-fourth of the unit cell is used for FE modeling, the FE model consists of a rectangular prism with dimensions x = 100 mm, y = 100 mm, and z = 10 mm, with an embedded one-fourth portion of continuous fiber (PALF, Palm, or Alfa fiber) of radius rf at one of the square cube's corners, which is the center of the tubular fiber, where the length of the fiber is taken as 10 mm. As a result, the analysis will be faster and computational time will be lowered.

The radius of the fiber is calculated for various weight percentages of the fibers. The weight percentages are converted into volume fractions. Four different volume fractions of fiber have been studied for the analysis, ranging from 15% to 24% with an increment of 3% of the volume fraction of the fiber. Thus, the following (17) is obtained:

$$rf = \sqrt{\frac{Vf \times 100^2 \times 4}{\pi}} \tag{17}$$

where: rf is the radius of the cylindrical fiber Vf is the volume fraction of the fiber.

Figure 4 gives an example of the converged mesh models of a composite at different volume fractions of natural fibers.
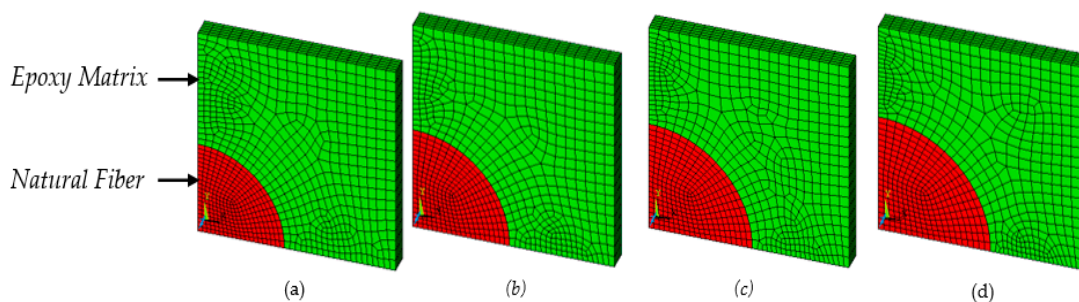

Figure 4. Converged mesh models of composite (RVE dimension) at: (**a**) 15%; (**b**) 18%; (**c**) 21% and (**d**) 24% of volume fraction of natural fibers.

2.2.4. Loading and Boundary Conditions

The finite element model is subjected to boundary conditions that force it to behave as if it were a component of the entire array of composite materials. One-eighth of the unit cell is modeled in the analysis due to symmetry in loads, geometry, and boundary conditions. The mentioned symmetrical boundary conditions were unit displacement from the symmetry of the problem. An overlapped volume connection is used between the fiber and the matrix.

A value displacement load of 1 mm is applied to the face to establish a uniaxial state of stress in that direction, allowing the Young's modulus and Poisson's ratio of the resultant composite to be predicted using simple Hook's law. The uniaxial state of displacement on the surface z = 10 mm is used to estimate longitudinal Young's modulus E_{11} and Poisson's Ratio v_{12}.

The area at x = 100 mm is exposed to a uniaxial displacement condition to predict transverse Young's modulus E_{22}. A uniaxial stress condition is given to the area at y = 100 mm to predict shear modulus G_{12}. In Figure 5, it is possible to see the boundary conditions.
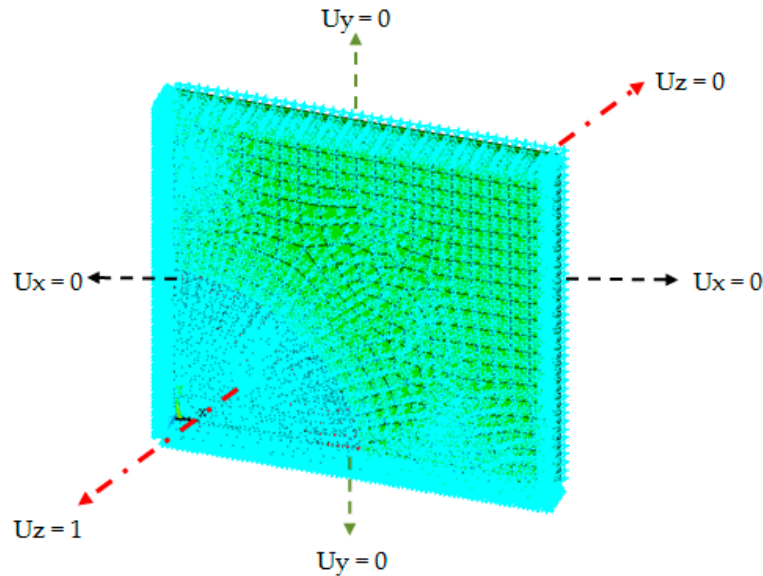

Figure 5. Loading and boundary conditions of the numerical model for predicting E_{11}.

A mesh convergence is performed on the longitudinal Young's modulus of PALF at a 15% volume fraction to verify the accuracy of our findings. It is clear that we have arrived at a converged solution. The results of the FEA model are independent of mesh size.

The results of the convergence analyses based on changing the number of elements in the mesh are summarized in Figure 6.
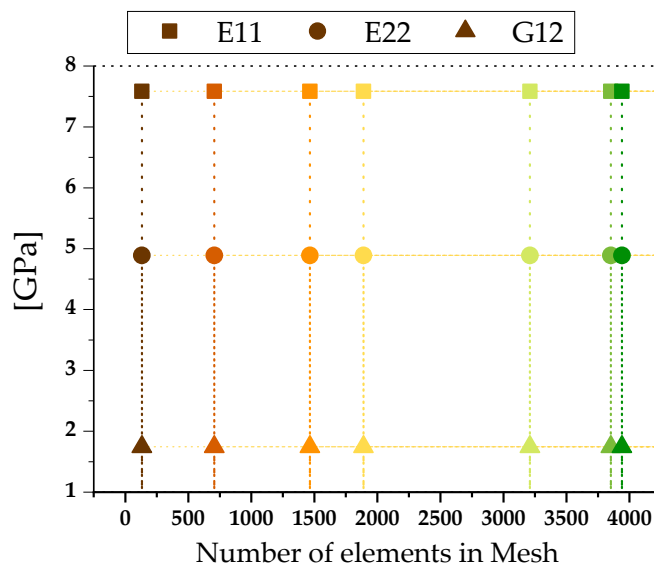

Figure 6. Mesh convergence analysis for finite elements of: E_{11}, E_{22} and G_{12} at 15% of volume fraction of natural fiber.

For varied mesh sizes, Figure 6 illustrates a fairly similar study for: longitudinal Young's modulus E_{11}, Transverse Young's modulus E_{22} and shear modulus G_{12}. It demonstrates that the FEA model's results are unaffected by the number of elements in the mesh.

By choosing a unit value of applied strain, and once the problem defined by the boundary conditions is solved, it is possible to compute the stress field σ_α, whose average gives the required components of the elastic matrix, one column at a time, as:

$$C_{\alpha\beta} = \overline{\sigma}_\alpha = \frac{1}{V} \int_V \sigma_{\alpha(x_1,\ x_2,x_3)dV} \quad \text{with} \quad \epsilon_\beta^0 = 1 \tag{18}$$

where: $\alpha, \beta = 1$. The integral sin (18) is evaluated within each finite element using the Gauss–Legendre quadrature. Commercial programs, such as ANSYS®, have the capability to compute the average stress and volume, element by element [42].

For the elastic domain:

$$W = \int_0^\varepsilon \sigma d\varepsilon = \frac{1}{2}\sigma\varepsilon = \frac{\sigma^2}{2E} \tag{19}$$

3. Results and Discussion

The results of the analytical models developed for the fiber reinforced composite are compared to the experimental results for the PALF/epoxy unidirectional composite from Rakesh's study [13], as shown in figures below.

The predicted results for all the analyzed models agree with the experimental data for composites (PALF/epoxy) with varying volume fractions. To characterize the tensile properties, unidirectional composite specimens were manufactured according to the necessary standard. The specimens were 160 mm, 12.5 mm, and 3 mm in size, respectively. For each volume fraction of the fiber, five identical samples were manufactured, and all specimens were examined using an electronic tensometer at a strain rate of 0.5 mm/min. Single fiber testing was used to characterize the PALF fiber's tensile modulus according to the ASTM D3379 standard. A total of 23 specimens were evaluated in order to obtain an exact figure for the PALF fiber's property [13]. The composites' longitudinal Young's modulus increases as the volume fraction of fiber rises, as can be shown in Figure 7.
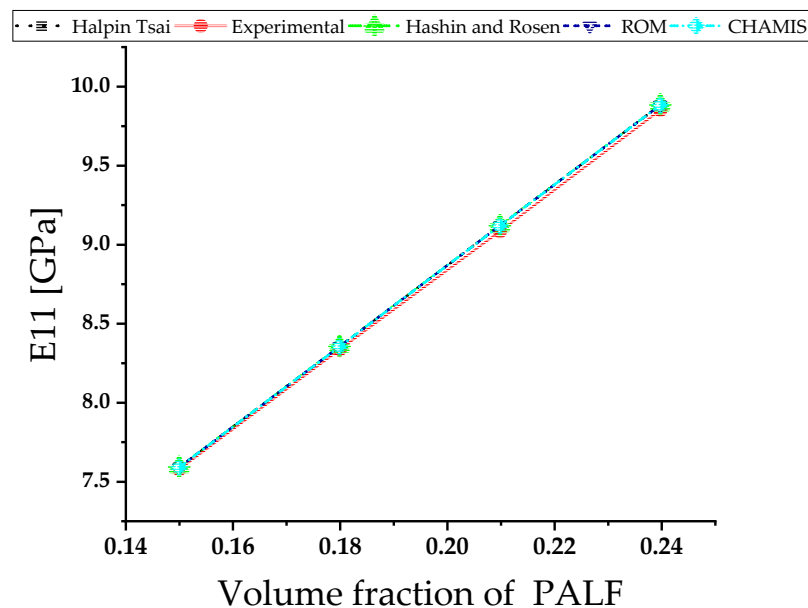

Figure 7. Comparison (analytical vs. exp) of Longitudinal Young's modulus E_{11} of PALF/epoxy in terms of volume fractions.

Figure 8 shows that the transverse Young's modulus E_{22} of composites increases along with the volume fraction of fiber, but the increment is lower when compared with the magnitude of E_{11}. The closest agreement with the experimental results belongs to Halpin Tsai model.
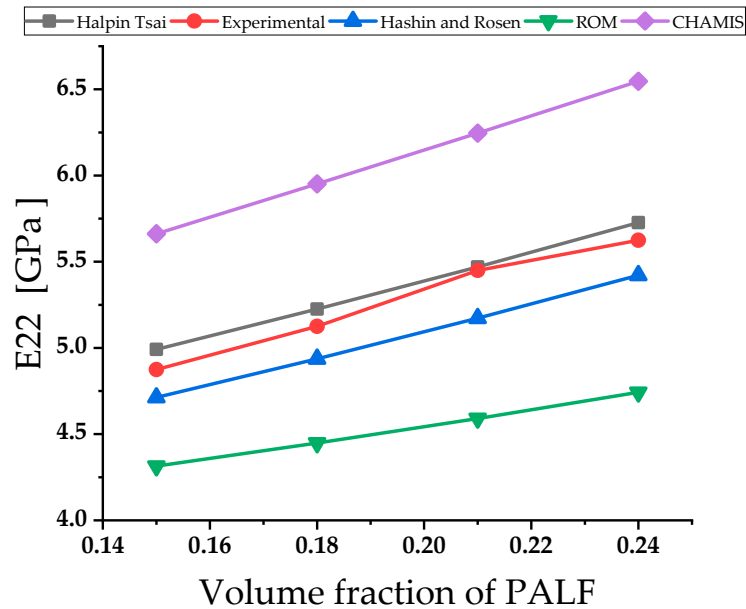

Figure 8. Transverse Young's modulus E_{22} of PALF /epoxy in terms of different volume fractions of fiber.

The analytical analysis results are compared to the experimental data in Figure 9. When compared to experimental data, the results generated by the analytical model of Chamis offer remarkably similar results.
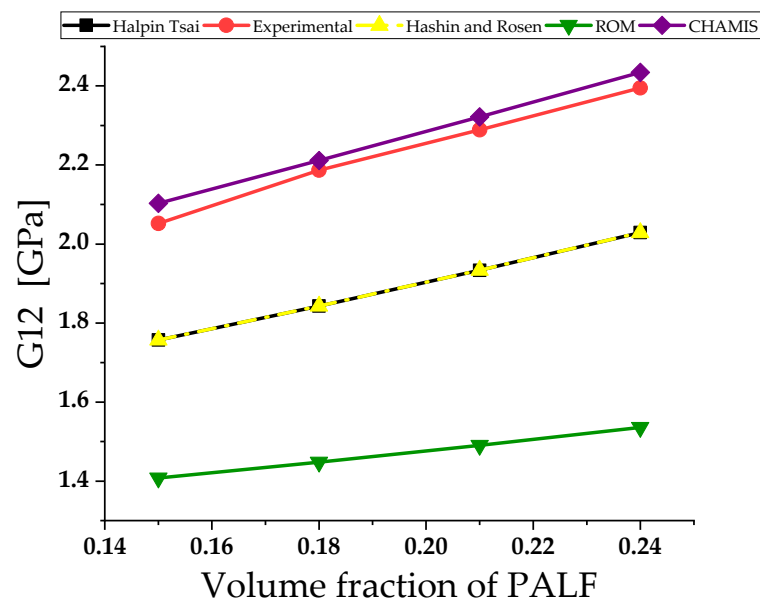

Figure 9. The comparison of shear modulus G_{12} of PALF/epoxy in terms of volume fractions.

It can be seen that the predicted values of the Poisson's ratio v_{12} for all tested models are in good agreement; this is illustrated in Figure 10.
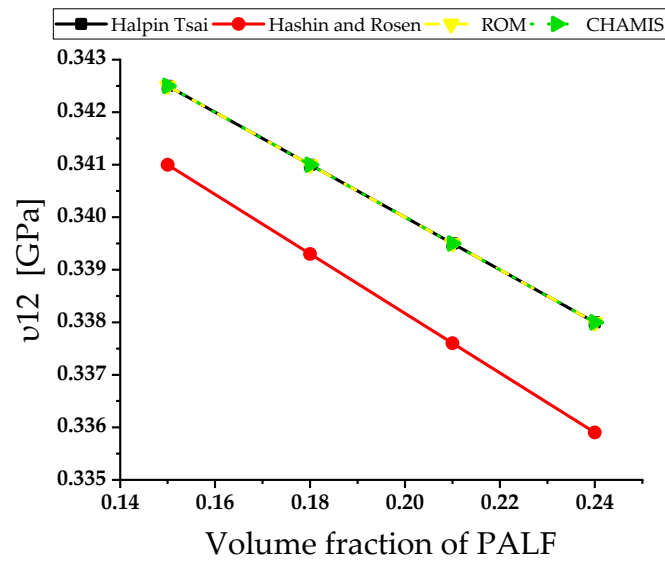
Figure 10. The Poisson's ratio v_{12} of PALF/epoxy in terms of V_F.

The first analytical part permitted us to select the analytical method that allows us to have mechanical properties that best converge with the experimental results. To forecast E_{11} and E_{22}, the Halpin-Tsai approach was chosen. For G_{12}, it is Chamis, and for v_{12}, it is ROM. A FEM approach is established and compared with the results of the analytical analysis in order to strengthen our prediction.

The variation of E_{11} and E_{22} as a function of the volume fraction of natural fibers, obtained by Halpin-Tsai and numerical analysis.

For all composites with varied V_F, the predicted results of FEM for E_{11} are in agreement with the analytical results. These examples are depicted in Figure 11. The prediction of the longitudinal modulus shows that the composite based on PALF fibers presents the best behavior in tension.
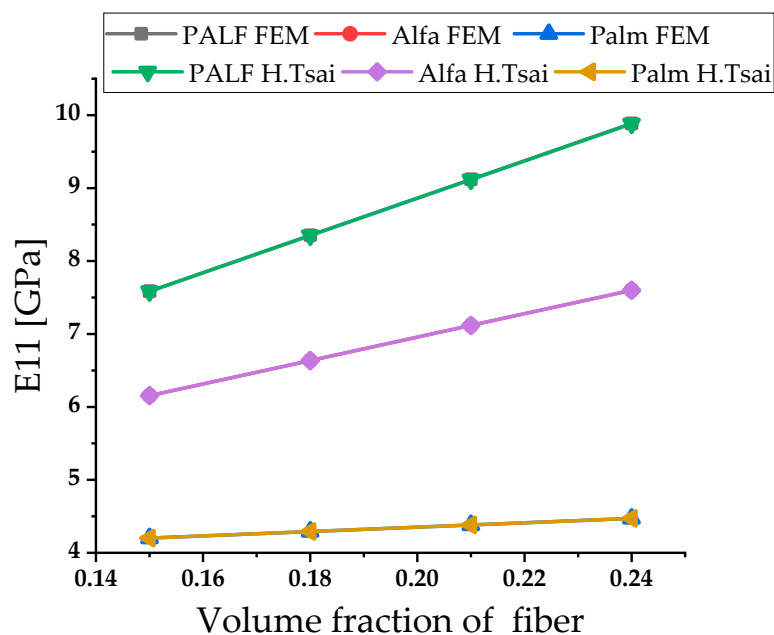

Figure 11. Predicted analytical (Halpin–Tsai model) and numerical results for E_{11} in terms of V_F.

The FEM anticipated results are in good correlation with the analytical results. Figure 12 shows a comparison of the results obtained for E_{22} using the FEM and the

analytical analysis. The prediction of the transverse modulus show that the composite based on PALF fibers presents the best behavior in compression.
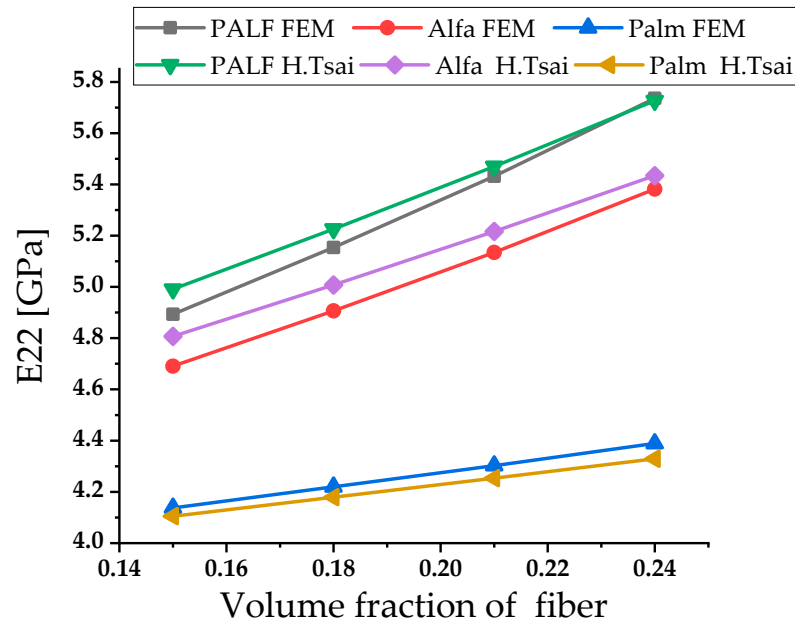

Figure 12. Predicted analytical (Halpin–Tsai model) and numerical results for E_{22} in terms of V_F.

Chamis and numerical analysis were used to determine the variation of G_{12} as a function of the volume fraction of natural fiber. When compared to analytical results, the numerical approach of finite element analysis yields good results, this can be found in Figure 13. The prediction of the shear modulus shows that the composite based on PALF fibers presents the best behavior in shear.
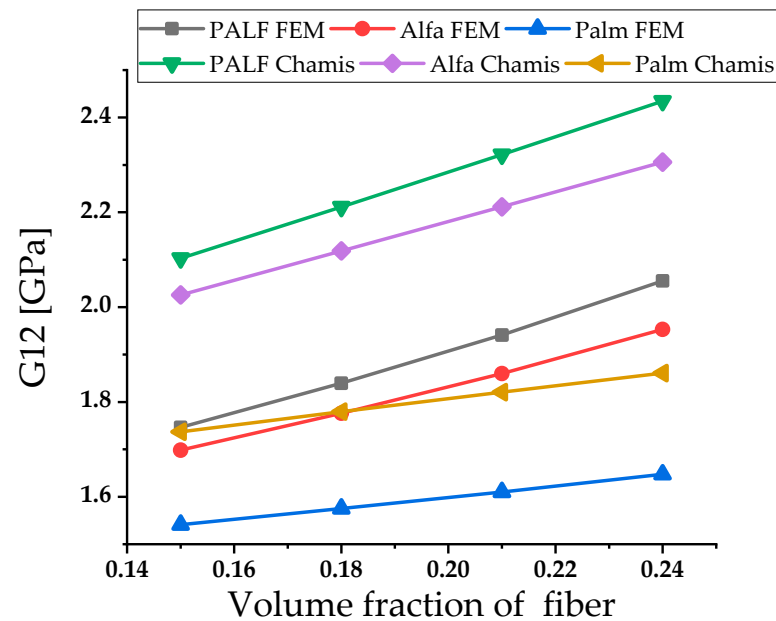

Figure 13. Predicted analytical (Chamis model) and numerical results for Shear Modulus G_{12} in terms of V_F.

Concerning the major Poisson's ratio, the results were obtained only from the ROM model and the FEM. Concerning the Poisson's ratios, the obtained results of the analytical models show that the Alfa/epoxy has the highest Poisson's ratio compared to PALF/epoxy

and palm/epoxy. Figure 14 shows that for the major Poisson's ratio v_{12}, all analytical and numerical models correlate well with each other.
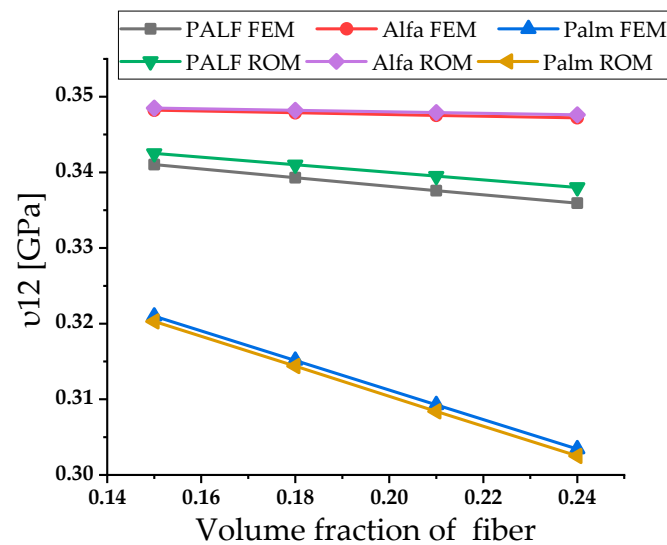

Figure 14. Predicted analytical (ROM model) and numerical results of Poisson's ratios v_{12} in terms of V_F.

4. Conclusions

In the present work, models were developed and used analytical and numerical methods to predict some mechanical properties of composite layers based on natural fibers. To accomplish these goals, we used four micromechanical analytical models, namely the Halpin–Tsai, the Chamis, the Hashin vs. Rosen, and the ROM. The analytical results were compared to the numerical simulations (FEM) and experimental data. The analyzed composites have a matrix of epoxy resin which is reinforced by the natural fibers, PALF, DB date palm tree fiber and Alfa fiber.

Based on this study, it is possible to summarize the following conclusions:

- The change in volume fraction of fiber has a significant effect on elastic properties.
- The Young's modulus rises in tandem with the reinforcement weight percentage.
- The Poisson's ratio decreases as the weight fraction of reinforcement increases.
- The shear modulus is calculated using the analytical expression, and it is also increasing along with the reinforcement.
- The mechanical properties of E_{11}, E_{22}, G_{12}, v_{12} determined by the analytical micromechanical models agree with the experimental results.
- The analytical micromechanical models allow us to select the most appropriate theory used to determine the mechanical properties of PALF fibers that best fits to the experimental results. To forecast E_{11} and E_{22}, the Halpin–Tsai approach was chosen. For G_{12}, it is Chamis, and for v_{12}, it is ROM.
- The most appropriate theory was used with the FEM model to predict the mechanical properties of skin layers based on PALF, date palm and Alfa fibers, where the results are in efficient consensus.
- The present work shows the successful prediction of elastic properties of composites by Finite Element Analysis.

However, the predictions for the elastic properties of the three fiber-based eco-composites showed a strong dispersion in terms of stiffness. Nevertheless, in future works, it is possible to test several fiber combinations to determine the best combination that has high values for mechanical properties in all directions. With this information, it is feasible to manufacture the composite without trying each combination with experimental tests, which will be a costly and time-intensive process.

Conflicts of Interest: The authors declare no conflict of interest.

References

1. Maizia, A.; Hocine, A.; Dehmous, H.; Chapelle, D. Prediction of reliability analysis of composite tubular structure under hygro-thermo-mechanical loading. *Mech. Adv. Mater. Struct.* **2019**, *26*, 372–379. [CrossRef]
2. Chapelle, D.; Hocine, A.; Carbillet, S.; Boubakar, M. Analysis of intermetallic swelling on the behavior of a hybrid solution for compressed hydrogen storage–Part II: Finite element method simulation. *Mater. Des.* **2012**, *36*, 459–469. [CrossRef]
3. Tarlochan, F. Sandwich structures for energy absorption applications: A review. *Materials* **2021**, *14*, 4731. [CrossRef]
4. Sanjay, M.R.; Arpitha, G.R.; Naik, L.L.; Gopalakrishna, K.; Yogesha, B. Applications of natural fibers and its composites: An overview. *Nat. Resour.* **2016**, *7*, 108–114. [CrossRef]
5. Xia, M.; Takayanagi, H.; Kemmochi, K. Bending behavior of filament-wound fiber-reinforced sandwich pipes. *Compos. Struct.* **2002**, *56*, 201–210. [CrossRef]
6. Hastie, J.C.; Kashtalyan, M.; Guz, I.A. Analysis of filament-wound sandwich pipe under combined internal pressure and thermal load considering restrained and closed ends. *Int. J. Press. Vessel. Pip.* **2021**, *191*, 104350. [CrossRef]
7. Lotfi, A.; Li, H.; Dao, D.V.; Prusty, G. Natural fiber–reinforced composites: A review on material, manufacturing, and machinability. *J. Thermoplast. Compos. Mater.* **2019**, *34*, 238–284. [CrossRef]
8. CoDyre, L.; Fam, A. Axial Strength of Sandwich Panels of Different Lengths with Natural Flax-Fiber Composite Skins and Different Foam-Core Densities. *J. Compos. Constr.* **2017**, *21*, 04017042. [CrossRef]
9. Sadeghian, P.; Hristozov, D.; Wroblewski, L. Experimental and analytical behavior of sandwich composite beams: Comparison of natural and synthetic materials. *J. Sandw. Struct. Mater.* **2018**, *20*, 287–307. [CrossRef]
10. Alhijazi, M.; Zeeshan, Q.; Qin, Z.; Safaei, B.; Asmael, M. Finite element analysis of natural fibers composites: A review. *Nanotechnol. Rev.* **2020**, *9*, 853–875. [CrossRef]
11. Sailesh, A.; Arunkumar, R.; Saravanan, S. Mechanical properties and wear properties of kenaf–aloe vera–jute fiber reinforced natural fiber composites. *Mater. Today: Proc.* **2018**, *5*, 7184–7190. [CrossRef]
12. El-Abbassi, F.E.; Assarar, M.; Ayad, R.; Bourmaud, A.; Baley, C. A review on alfa fibre (*Stipa tenacissima* L.): From the plant architecture to the reinforcement of polymer composites. *Compos. Part A: Appl. Sci. Manuf.* **2019**, *128*, 105677. [CrossRef]
13. Potluri, R.; Diwakar, V.; Venkatesh, K.; Reddy, B.S. Analytical model application for prediction of mechanical properties of natural fiber reinforced composites. *Mater. Today: Proc.* **2018**, *5*, 5809–5818. [CrossRef]
14. Ashwini, K.; Rao, C.M. Design and analysis of leaf spring using various composites—An overview. *Mater. Today: Proc.* **2018**, *5*, 5716–5721. [CrossRef]
15. Dragonetti, R.; Napolitano, M.; Boccarusso, L.; Durante, M. A study on the sound transmission loss of a new lightweight hemp/bio-epoxy sandwich structure. *Appl. Acoust.* **2020**, *167*, 107379. [CrossRef]
16. Sapiai, N.; Jumahat, A.; Mahmud, J. Mechanical properties of functionalised CNT filled kenaf reinforced epoxy composites Mechanical properties of functionalised CNT fi lled kenaf reinforced epoxy composites. *Mater. Res. Express* **2018**, *5*, 045034. [CrossRef]
17. Elzayady, N.E.; Elghandour, E.I. Fracture resistance of composite structurs from hemp bio-fibers. *J. Adv. Eng. Trends* **2021**, *40*, 137–147. [CrossRef]
18. Boria, S.; Raponi, E.; Sarasini, F.; Tirillò, J.; Lampani, L. Green sandwich structures under impact: Experimental vs numerical analysis. *Procedia Struct. Integr.* **2018**, *12*, 317–329. [CrossRef]
19. Safri, S.N.A.; Sultan, M.T.H.; Jawaid, M.; Jayakrishna, K. Impact behaviour of hybrid composites for structural applications: A review. *Compos. Part B: Eng.* **2018**, *133*, 112–121. [CrossRef]
20. Kiruthika, A. A review on physico-mechanical properties of bast fibre reinforced polymer composites. *J. Build. Eng.* **2017**, *9*, 91–99. [CrossRef]
21. Zhang, K.-L.; Zhang, J.-Y.; Hou, Z.-L.; Bi, S.; Zhao, Q.-L. Multifunctional broadband microwave absorption of flexible graphene composites. *Carbon* **2019**, *141*, 608–617. [CrossRef]
22. Alsubari, S.; Zuhri, M.Y.M.; Sapuan, S.M.; Ishak, M.R.; Ilyas, R.A.; Asyraf, M.R.M. Potential of natural fiber reinforced polymer composites in sandwich structures: A review on its mechanical properties. *Polymers* **2021**, *13*, 423. [CrossRef] [PubMed]
23. Monteiro, S.N.; Lopes, F.P.D.; Ferreira, A.S.; Nascimento, D.C.O. Natural-fiber polymer-matrix composites: Cheaper, tougher, and environmentally friendly. *JOM* **2009**, *61*, 17–22. [CrossRef]
24. Nurazzi, M.; Khalina, A.; Laila, D. A review: Fibres, Polymer Matrices and Composites. *Pertanika J. Sci. Technol.* **2017**, *25*, 1085–1102.

25. Lee, C.; Khalina, A.; Lee, S. Importance of interfacial adhesion condition on characterization of plant-fiber-reinforced polymer composites: A review. *Polymers* **2021**, *13*, 438. [CrossRef]

26. Campilho, R.D.S. *Natural Fiber Composites*; CRC Press: London, UK; New York, NY, USA, 2016; Volume 49.

27. Monti, C. *Arthur Élaboration et Caractérisation d'une De, Structure Composite Sandwiche à Base Naturels*; l'Université du Maine: Le Mans, France, 2016.

28. Ali, A.; Shaker, K.; Nawab, Y.; Jabbar, M.; Hussain, T.; Militky, J.; Baheti, V. Hydrophobic treatment of natural fibers and their composites—A review. *J. Ind. Text.* **2018**, *47*, 2153–2183. [CrossRef]

29. Pan, Y.; Iorga, L.; Pelegri, A.A. Numerical generation of a random chopped fiber composite RVE and its elastic properties. *Compos. Sci. Technol.* **2008**, *68*, 2792–2798. [CrossRef]

30. Benabbes, A.; Siad, L.; Dormieux, L.; Liu, W.K.; Barlat, F.; Moon, Y.H.; Lee, M.G. A homogenization approach to the yield strength of spherical powder compacts. *AIP Conf. Proc.* **2010**, *1252*, 681. [CrossRef]

31. Porfiri, M.; Gupta, N. Effect of volume fraction and wall thickness on the elastic properties of hollow particle filled composites. *Compos. Part B Eng.* **2009**, *40*, 166–173. [CrossRef]

32. Migneault, S.; Koubaa, A.; Erchiqui, F.; Chaala, A.; Englund, K.; Wolcott, M.P. Application of micromechanical models to tensile properties of wood–plastic composites. *Wood Sci. Technol.* **2011**, *45*, 521–532. [CrossRef]

33. Tserpes, K.; Tzatzadakis, V.; Bachmann, J. Electrical Conductivity and Electromagnetic Shielding Effectiveness of Bio-Composites. *J. Compos. Sci.* **2020**, *4*, 28. [CrossRef]

34. Al-Fatlawi, A.; Jármai, K.; Kovács, G. Optimal design of a fiber-reinforced plastic composite sandwich structure for the base plate of aircraft pallets in order to reduce weight. *Polymers* **2021**, *13*, 834. [CrossRef] [PubMed]

35. Feng, Y.; Jia, B.; Wang, X.; Zhang, M.; Zhu, Z. Research on microscopic properties of tibw/tc4 composites for drilling process. *Materials* **2019**, *12*, 2112. [CrossRef] [PubMed]

36. Craveiro, D.S.; Loja, M.A.R. An assessment of thick nanocomposite plates' behavior under the influence of carbon nanotubes agglomeration. *J. Compos. Sci.* **2021**, *5*, 41. [CrossRef]

37. Kriwet, A.; Stommel, M. Arbitrary-Reconsidered-Double-Inclusion (ARDI) model to describe the anisotropic, viscoelastic stiffness and damping of short fiber-reinforced thermoplastics. *J. Compos. Sci.* **2020**, *4*, 37. [CrossRef]

38. Djebloun, Y.; Hecini, M.; Djoudi, T.; Guerira, B. Experimental determination of elastic modulus of elasticity and Poisson's coefficient of date palm tree fiber. *J. Nat. Fibers* **2019**, *16*, 357–367. [CrossRef]

39. Imen, R.; Wadhah, S.; Rached, B.Y. Identification de la loi de comportement des matériaux composites à fibres organiques (*Stipa tenacissima* L) Identification of the behaviour law of organic fibre composite materials 5 éme Conférence. *Int. Des. Energ. Renouv. Proc. Eng. Technol.* **2017**, *31*, 37–42.

40. Asim, M.; Abdan, K.; Jawaid, M.; Nasir, M.; Dashtizadeh, Z.; Ishak, M.R.; Hoque, M.E. A Review on Pineapple Leaves Fibre and Its Composites. *Int. J. Polym. Sci.* **2015**, *2015*, 950567. [CrossRef]

41. Younes, R.; Hallal, A.; Fardoun, F.; Hajj, F. Comparative review study on elastic properties modeling for unidirectional composite materials. *Compos. Prop.* **2012**, *17*, 391–408. [CrossRef]

42. Barbero, E.J. *Finite Element Analysis of Composite Materials Using Ansys*, 2nd ed.; CRC Press: Boca Raton, FL, USA, 2013.